Flexible modulation of plasmon-induced transparency in a strongly coupled graphene grating-sheet system

Weiwei Luo,[1,2,3] **Wei Cai,**[1,2,3,4] **Yinxiao Xiang,**[1,2,3] **Lei Wang,** [1,2,3] **Mengxin Ren,**[1,2,3,5] **Xinzheng Zhang,**[1,2,3] **and Jingjun Xu**[1,2,3,6]

[1]*The Key Laboratory of Weak-Light Nonlinear Photonics, Ministry of Education, School of Physics and TEDA Applied Physics Institute, Nankai University, Tianjin 300457, China*
[2]*Synergetic Innovation Center of Chemical Science and Engineering, Tianjin 300457, China*
[3]*Collaborative Innovation Center of Extreme Optics, Shanxi University, Taiyuan, Shanxi 030006, China*
[4]*weicai@nankai.edu.cn*
[5]*renmengxin@nankai.edu.cn*
[6]*jjxu@nankai.edu.cn*

Abstract: General actively tunable near-field plasmon-induced transparency (PIT) systems based on couplings between localized plasmon resonances of graphene nanostructures not only suffer from interantenna separations of smaller than 20 nm, but also lack switchable effect about the transparency window. Here, the performance of an active PIT system based on graphene grating-sheet with near-field coupling distance of more than 100 nm is investigated in mid-infrared. The transparency window in spectrum is analyzed objectively and proved to be more likely stemmed from Aulter-Townes splitting. The proposed system exhibits flexible tunability in slow-light and electro-optical switches, promising for practical active photonic devices.

OCIS codes: (240.6680) Surface plasmons; (250.5403) Plasmonics; (260.5740) Resonance.

References and links

1. K. S. Novoselov, A. K. Geim, S. V. Morozov, D. Jiang, Y. Zhang, S. V. Dubonos, I. V. Grigorieva, and A. A. Firsov, "Electric field effect in atomically thin carbon films," Science **306**, 666–669 (2004).
2. E. H. Hwang and S. Das Sarma, "Dielectric function, screening, and plasmons in two-dimensional graphene," Phys. Rev. B **75**, 205418 (2007).
3. M. Jablan, H. Buljan, and M. Soljačić, "Plasmonics in graphene at infrared frequencies," Phys. Rev. B **80**, 245435 (2009).
4. L. Ju, B. Geng, J. Horng, C. Girit, M. Martin, Z. Hao, H. A. Bechtel, X. Liang, A. Zettl, Y. R. Shen, and F. Wang, "Graphene plasmonics for tunable terahertz metamaterials," Nat. Nanotechnol. **6**, 630–634 (2011).
5. F. H. L. Koppens, D. E. Chang, and F. J. García de Abajo, "Graphene plasmonics: A platform for strong light-matter interactions," Nano Lett. **11**, 3370–3377 (2011).
6. J. Chen, M. Badioli, P. Alonso-Gonzalez, S. Thongrattanasiri, F. Huth, J. Osmond, M. Spasenovic, A. Centeno, A. Pesquera, P. Godignon, A. Zurutuza Elorza, N. Camara, F. J. G. de Abajo, R. Hillenbrand, and F. H. L. Koppens, "Optical nano-imaging of gate-tunable graphene plasmons," Nature **487**, 77–81 (2012).
7. Z. Fei, A. S. Rodin, G. O. Andreev, W. Bao, A. S. McLeod, M. Wagner, L. M. Zhang, Z. Zhao, M. Thiemens, G. Dominguez, M. M. Fogler, A. H. C. Neto, C. N. Lau, F. Keilmann, and D. N. Basov, "Gate-tuning of graphene plasmons revealed by infrared nano-imaging," Nature **487**, 82–85 (2012).
8. A. N. Grigorenko, M. Polini, and K. S. Novoselov, "Graphene plasmonics," Nat. Photonics **6**, 749–758 (2012).
9. V. W. Brar, M. S. Jang, M. Sherrott, J. J. Lopez, and H. A. Atwater, "Highly confined tunable mid-infrared plasmonics in graphene nanoresonators," Nano Lett. **13**, 2541–2547 (2013).

#257415 Received 14 Jan 2016; revised 2 Mar 2016; accepted 3 Mar 2016; published 7 Mar 2016

10. Z. Fang, S. Thongrattanasiri, A. Schlather, Z. Liu, L. Ma, Y. Wang, P. M. Ajayan, P. Nordlander, N. J. Halas, and F. J. García de Abajo, "Gated tunability and hybridization of localized plasmons in nanostructured graphene," ACS Nano **7**, 2388–2395 (2013).
11. H. Yan, T. Low, W. Zhu, Y. Wu, M. Freitag, X. Li, F. Guinea, P. Avouris, and F. Xia, "Damping pathways of mid-infrared plasmons in graphene nanostructures," Nat. Photonics **7**, 394–399 (2013).
12. P. Alonso-Gonzalez, A. Y. Nikitin, F. Golmar, A. Centeno, A. Pesquera, S. Velez, J. Chen, G. Navickaite, F. Koppens, A. Zurutuza, F. Casanova, L. E. Hueso, and R. Hillenbrand, "Controlling graphene plasmons with resonant metal antennas and spatial conductivity patterns," Science **344**, 1369–1373 (2014).
13. A. Woessner, M. B. Lundeberg, Y. Gao, A. Principi, P. Alonso-Gonzaolez, M. Carrega, K. Watanabe, T. Taniguchi, G. Vignale, M. Polini, J. Hone, R. Hillenbrand, and F. H. L. Koppens, "Highly confined low-loss plasmons in graphene-boron nitride heterostructures," Nat. Mater. **14**, 421–425 (2015).
14. S. Zhang, D. A. Genov, Y. Wang, M. Liu, and X. Zhang, "Plasmon-induced transparency in metamaterials," Phys. Rev. Lett. **101**, 047401 (2008).
15. N. Liu, L. Langguth, T. Weiss, J. Kastel, M. Fleischhauer, T. Pfau, and H. Giessen, "Plasmonic analogue of electromagnetically induced transparency at the drude damping limit," Nat. Mater. **8**, 758–762 (2009).
16. R. D. Kekatpure, E. S. Barnard, W. Cai, and M. L. Brongersma, "Phase-coupled plasmon-induced transparency," Phys. Rev. Lett. **104**, 243902 (2010).
17. J. Gu, R. Singh, X. Liu, X. Zhang, Y. Ma, S. Zhang, S. A. Maier, Z. Tian, A. K. Azad, H. T. Chen, A. J. Taylor, J. Han, and W. Zhang, "Active control of electromagnetically induced transparency analogue in terahertz metamaterials," Nat. Commun. **3**, 1151 (2012).
18. K. Boller, A. Imamolu, and S. E. Harris, "Observation of electromagnetically induced transparency," Phys. Rev. Lett. **66**, 2593–2596 (1991).
19. M. Fleischhauer, A. Imamoglu, and J. P. Marangos, "Electromagnetically induced transparency: optics in coherent media," Rev. Mod. Phys. **77**, 633–673 (2005).
20. H. Cheng, S. Q. Chen, P. Yu, X. Y. Duan, B. Y. Xie, and J. G. Tian, "Dynamically tunable plasmonically induced transparency in periodically patterned graphene nanostrips," Appl. Phys. Lett. **103**, 203112 (2013).
21. X. Shi, D. Han, Y. Dai, Z. Yu, Y. Sun, H. Chen, X. Liu, and J. Zi, "Plasmonic analog of electromagnetically induced transparency in nanostructure graphene," Opt. Express **21**, 28438–43 (2013).
22. J. Ding, B. Arigong, H. Ren, M. Zhou, J. Shao, M. Lu, Y. Chai, Y. Lin, and H. Zhang, "Tuneable complementary metamaterial structures based on graphene for single and multiple transparency windows," Sci. Rep. **4**, 6128 (2014).
23. L. Wang, W. Cai, W. Luo, Z. Ma, C. Du, X. Zhang, and J. Xu, "Mid-infrared plasmon induced transparency in heterogeneous graphene ribbon pairs," Opt. Express **22**, 32450–32456 (2014).
24. C. Zeng, J. Guo, and X. M. Liu, "High-contrast electro-optic modulation of spatial light induced by graphene-integrated fabry-perot microcavity," Appl. Phys. Lett. **105**, 121103 (2014).
25. R. W. Yu, R. Alaee, F. Lederer, and C. Rockstuhl, "Manipulating the interaction between localized and delocalized surface plasmon-polaritons in graphene," Phys. Rev. B **90**, 085409 (2014).
26. S. H. Autler and C. H. Townes, "Stark effect in rapidly varying fields," Phys. Rev. **100**, 703–722 (1955).
27. P. M. Anisimov, J. P. Dowling, and B. C. Sanders, "Objectively discerning autler-townes splitting from electromagnetically induced transparency," Phys. Rev. Lett. **107**, 163604 (2011).
28. B. Peng, Ş. K. Özdemir, W. Chen, F. Nori, and L. Yang, "What is and what is not electromagnetically induced transparency in whispering-gallery microcavities," Nat. Commun. **5**, 5082 (2014).
29. E. J. Wagenmakers, "Model selection and multimodel inference: A practical information-theoretic approach," J. Math. Psych. **47**, 580–586 (2003).
30. B. Wunsch, T. Stauber, F. Sols, and F. Guinea, "Dynamical polarization of graphene at finite doping," New J. Phys. **8**, 318 (2006).
31. P. Tassin, L. Zhang, R. Zhao, A. Jain, T. Koschny, C. M. Soukoulis, "Electromagnetically induced transparency and absorption in metamaterials: the radiating two-oscillator model and its experimental confirmation," Phys. Rev. Lett. **109**, 187401 (2012).
32. A. Y. Nikitin, T. Low, and L. Martin-Moreno, "Anomalous reflection phase of graphene plasmons and its influence on resonators," Phys. Rev. B **90**, 041407 (2014).
33. L. P. Du, D. Y. Tang, and X. C. Yuan, "Edge-reflection phase directed plasmonic resonances on graphene nanostructures," Opt. Express **22**, 22689–22698 (2014).
34. B. Zhao and Z. M. Zhang, "Strong plasmonic coupling between graphene ribbon array and metal gratings," ACS Photonics **2**, 1611–1618 (2015).

1. Introduction

Graphene has shown various interesting properties in mechanical, electric, and optical applications [1]. Interestingly, graphene is also a promising candidate plasmon material in the terahertz to mid-infrared spectral range. Graphene plasmons (GPs) have been extensively inves-

#257415 Received 14 Jan 2016; revised 2 Mar 2016; accepted 3 Mar 2016; published 7 Mar 2016

tigated theoretically and experimentally [2–13]. Compared to metal plasmonics, GPs possess higher confinement, longer relative propagating distances and easier electrostatic tunablility. The wavelengths of the GPs are about 10^2 times smaller than the wavelength in free space [3]. Therefore, the huge momentum mismatch between free space photons and GPs should be compensated in experiments, such as a metallic antenna like a near-field tip [6, 7] or a resonant rod on graphene [12] can be utilized to launch propagating GPs. Apart from propagating GPs, localized GPs and their coupling have also attracted considerable attention in recent years. In particular, plasmon-induced transparency (PIT) [14–17], as an analog of electromagnetically induced transparency (EIT) [18, 19] in atomic systems, has been demonstrated in graphene structures [20–23]. These active systems exhibit promising applications in integrated photonic circuits, including slow light devices, plasmonic switches and optical sensors.

Nevertheless, there are several drawbacks that are needed to be improved. Firstly, the proposed near-field coupling schemes [20–23] rely heavily on the strength of the coupling between constituent nanoantennas, which requires a distance control as small as 20 nm. Such spacings, not only require a precise lithographic control, but also restrict the access to the coupling medium between the antennas [16]. Besides, the transparency windows can only be tuned along spectrum instead of switchable, which blocks their practical applications in active photonic devices. As an alternative, phase coupled PIT schemes have also been proposed [24], where antennas couple with each other mediated by phase differences instead of near-field. However, in these systems, maximum transparency only occurs at certain separations on the order of light wavelength and the transparency windows are spectrally narrow, limiting their applications in compact photonic circuits. On the other hand, strong coupling between localized and propagating surface plasmons can also take place in graphene systems [25], which provides us a platform to investigate PIT in these systems.

Both EIT and Aulter-Townes splitting (ATS) [26–28] can lead to transparency windows in spectra. While EIT is the result of Fano resonance among different transition pathways, on the other hand, ATS corresponds to the splitting of energy levels caused by strong field-driven interactions. Clarifying whether a transparency window is due to EIT or ATS is important for understanding the physical process behind and for specific applications. The Akaike Information Criterion (AIC) [27–29] has been proved as an objective test to discern EIT from ATS in experimentally obtained transmission spectra of atom systems [27] and coupled microresonators [28]. Detailed analysis on the origin of transparency windows in graphene PIT systems is needed.

In this paper, we achieve PIT effects in mid-infrared based on the strong coupling between localized and propagating plasmonic modes in layered graphene ribbon-grating and continuous sheet systems. The large evanescent decay length of propagating GPs enables the observation of transparency window for the separation of 120 nm at 31.7 THz. In addition, analytical fitting is employed and the AIC method is proved efficiently to distinguish the transparency window, which is found caused by ATS instead of EIT. EIT-like coupling only occurs when the two coupled modes endure quite varied damping rates. The presented system is tested for slowing light, exhibiting large and spectrally tunable group delays at the transparency window. Benefitting from the detachment of coupling components, the transparency window can be electrically switched with large on/off ratio. Therefore, this flexibly tunable system promises practical applications in electro-optical switches and integrated photonic circuits.

2. Graphene PIT system

The geometry of the graphene grating-sheet hybrid system is illustrated in Fig. 1. The graphene grating has a period of Λ with ribbon width of W. In this paper, Λ is chosen as 300 nm and the distance between the grating and sheet is defined as D. The Fermi energies of the graphene

#257415 Received 14 Jan 2016; revised 2 Mar 2016; accepted 3 Mar 2016; published 7 Mar 2016

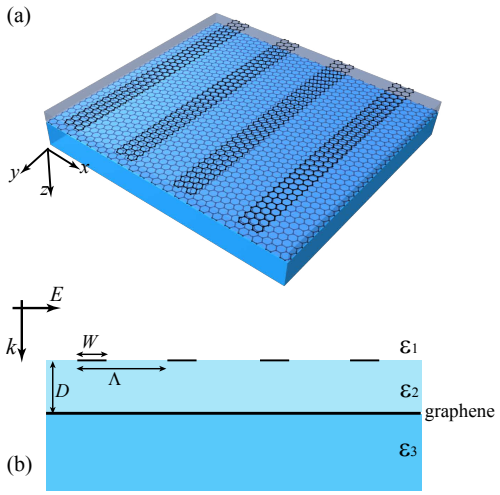

Fig. 1. Scheme of the proposed graphene grating/sheet system. (a) 3D view shows a graphene grating consisted of ribbons, beneath which lies a layer of graphene. (b) Cross-section of the structure in x-z plane. The period of graphene grating is Λ, and the width of ribbons is W. A plane wave incidents normally on the grating, with the electric field polarized along x direction. The separation of the two graphene layers is D. Surrounding dielectric constants are ε_1, ε_2 and ε_3, respectively.

grating and sheet are denoted by E_{F1} and E_{F2}, respectively. And the carrier mobilities are assigned to be $\mu_1 = \mu_2$=10000 cm^2/(V s).

The optical response of the designed structures is numerically simulated using COMSOL, which is based on finite element method. The optical conductivity of graphene is related to the Fermi energy E_F and carrier mobility μ, through random phase approximation (RPA) [30]. In the local limit, it follows

$$\begin{aligned}\sigma(\omega) &= \frac{2e^2\mathbb{T}}{\pi\hbar}\frac{i}{\omega+i\tau^{-1}}\log[2\cosh(\frac{E_F}{2K_B\mathbb{T}})] \\ &\quad + \frac{e^2}{4\hbar}\left[H(\omega/2)+\frac{4i\omega}{\pi}\int_0^\infty d\varepsilon\frac{H(\varepsilon)-H(\omega/2)}{\omega^2-4\varepsilon^2}\right],\end{aligned} \tag{1}$$

where

$$H(\varepsilon)=\frac{\sinh(\hbar\varepsilon/k_B\mathbb{T})}{\cosh(E_F/k_B\mathbb{T})+\cosh(\hbar\varepsilon/k_B\mathbb{T})}.$$

Here, $\tau=\mu E_F/ev_F^2$ is the intrinsic relaxation time, where $v_F\approx c/300$ is the Fermi velocity. Temperature $\mathbb{T}$ is set as 300 K.

To simplify analysis of the mechanism of coupling between graphene layers, ε_1, ε_2, and ε_3 are assumed to be 1, while the separation D is changed.

The dispersion of surface plasmon waves in the graphene sheet satisfies [3]

$$\frac{\varepsilon_2}{\sqrt{k_{GP}^2-\varepsilon_2 k_0^2}}+\frac{\varepsilon_3}{\sqrt{k_{GP}^2-\varepsilon_3 k_0^2}}=-\frac{i\sigma}{\omega\varepsilon_0}, \tag{2}$$

#257415 Received 14 Jan 2016; revised 2 Mar 2016; accepted 3 Mar 2016; published 7 Mar 2016

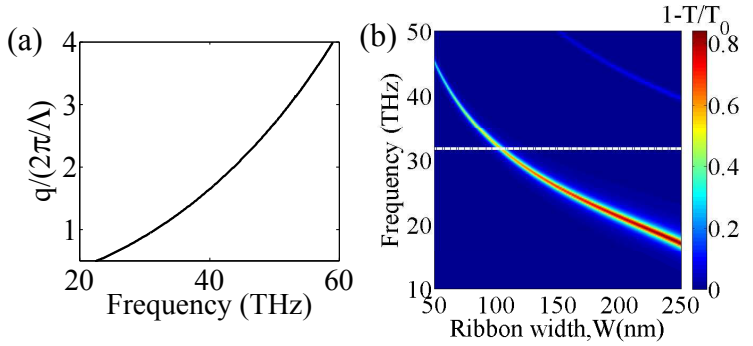

Fig. 2. (a) Dispersion relation of a suspended graphene sheet. The Fermi energy is 0.3 eV. (b) Extinction spectra for graphene grating of period 300 nm and Fermi energy of 0.3 eV. The widths of ribbons are changed from 50 to 250 nm. The dipolar plasmon resonance arises at 31.7 THz for W of 104 nm, as indicated by the dashed line.

where $k_0 = \omega/c$ is the wave vector in vacuum, and k_{GP} is the wave vector for the plasmons. As $\varepsilon_1 = \varepsilon_2 = \varepsilon_3 = 1$, the dispersion in the nonretarded regime ($k_{GP} \gg k_0$) is simplified as

$$k_{GP}(\omega) = \frac{2i\omega\varepsilon_0}{\sigma(\omega)}. \tag{3}$$

In Fig. 2(a), the dispersion relation of the real part of k_{GP} (represented by $q(\omega)$ here) is shown for E_{F2}=0.3 eV. For smaller D, i.e. the upper graphene grating is getting closer to the bottom graphene sheet, the propagating GPs in the sheet can be excited by the localized plasmon resonance (LPR) in the ribbon layer once the momentum conservation law is fulfilled as a result of the large wave momenta of near fields. In this way, the two layers are coupled efficiently. Moreover, due to the periodicity of graphene ribbons, only plasmon waves whose wave momenta satisfy

$$q\Lambda = m \cdot 2\pi \tag{4}$$

can exist. Integer m denotes the order. The frequencies of the first four supported SPPs modes can be deduced from Fig. 2(a), where the first one (FSP) exists at 31.7 THz (m=1). As shown in Fig. 2(b), the corresponding width of graphene ribbons should be 104 nm for the strongest near-field coupling between the LPR and FSP modes.

Figure 3(a) displays the transmission spectrum for the designed configuration, where a transparency window is obtained. Detailed field distributions at the two dips and peak are shown in Fig. 3(b). At ν_1 and ν_2, electrical fields are localized at the edges of graphene ribbons. The E_z distributions at ν_{12} in the bottom right panel of Fig. 3(b) imply the excitation of the FSP mode. Benefitting from the large decay length of the FSP mode [as depicted in Fig. 3(c)], the distance between graphene ribbon gating and graphene sheet is set as 120 nm, which is much larger than previous designs [20, 21].

3. Analytical fitting and AIC weight

In the coupling between the LPR and FSP modes, the LPR mode is excited by incident light, then electromagnetic energy is transported to the FSP mode. These interactions can be described by the coupled two-oscillator system as

$$\begin{aligned} \ddot{x_1} + \gamma_1\dot{x_1} + \omega_1^2 x_1 + \kappa^2 x_2 &= a_1 E_0 e^{i\omega t}, \\ \ddot{x_2} + \gamma_2\dot{x_2} + \omega_2^2 x_2 + \kappa^2 x_1 &= 0, \end{aligned} \tag{5}$$

#257415 Received 14 Jan 2016; revised 2 Mar 2016; accepted 3 Mar 2016; published 7 Mar 2016

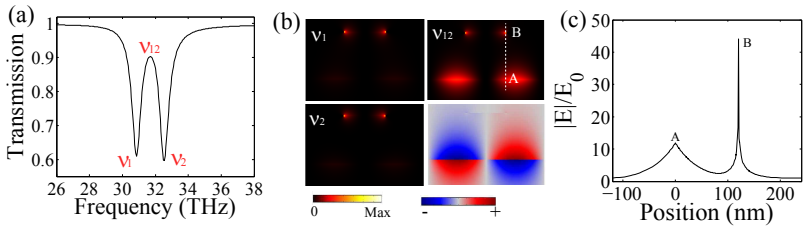

Fig. 3. (a) Transmission spectrum for the graphene grating-sheet system when the width of the ribbons is 104 nm. Here, D=120 nm. ν_1,ν_2 denote the frequencies at the left and right dip respectively. ν_{12} is the frequency at the PIT peak. (b) Simulated field distributions ($|E_z|^2$) for a unit cell at frequency of ν_1(top left), ν_2(bottom left) and ν_{12}(top right), respectively. A and B mark the planes of graphene sheet and grating, respectively. The bottom right panel shows the electric field distributions(E_z) at ν_{12}. (c) Normalized distributions of $|E|$ along the vertical line indicated in (b) at ν_{12}.

here, x_i, ω_i and γ_i are the resonance amplitude, frequency and damping rate of the resonance mode ($i = 1$ for the LPR mode and $i = 2$ for the FSP mode), respectively. κ is the coupling coefficient between the two resonance modes, and a_1 is a geometric parameter indicating the coupling strength of the LPR mode x_1 with electromagnetic field $E_0 e^{i\omega t}$.

The susceptibility χ of the system is proportional to the amplitude x_1 [14] and can be described as

$$\chi(\omega) = \chi_r + i\chi_i \propto \frac{\omega_2^2 - \omega^2 + i\gamma_2\omega}{(\omega_1^2 - \omega^2 + i\gamma_1\omega)(\omega_2^2 - \omega^2 + i\gamma_2\omega) - \kappa^4}. \tag{6}$$

Exact expression for transmission in the two-resonantor model has been described in a developed radiating model [31]. However, for the graphene plasmon system, a predigestion can be employed. Due to the large wave vector mismatch between GPs and far-field, the scattering of plasmons back into photons is very weak. As a result, the extinction cross section is dominated by dissipated energy in the system [5]. As the energy dissipation is proportional to the imaginary part of susceptibility χ_i, the transmission T can be described as $T(\omega) = 1 - g\chi_i(\omega)$ [22], where g is a geometric parameter related to the coupling strength between the resonant mode and the incident electromagnetic field.

Figure 4 displays the transmission spectra at different distances D by numerical calculations and analytical fittings, which reveal excellent agreements. One can find that the transparency windows gradually appear and broaden as D decreases. The fitted parameters are shown in the top panel of Fig. 5(a). With the decrease of D, the coupling strength κ experiences rapid increase due to the stronger near-field coupling.

Then, the AIC method is tested for the origin of the transparency windows at different coupling strengths. Given a parametric model, there is a unique set of parameters that minimize the Kullback-Leibler (K-L) distance between the model and the truth, where K-L distance defines the information lost when the model is used to approximate the truth. The AIC method defines a criterion to quantify information lost of the model g_i and is explained as $I_i = -2\log(L_i) + 2k_i$, where L_i is the the maximum likelihood for the candidate model and k_i the number of estimable parameters. Then the relative likelihood of the model g_i is expressed by the Akaike weight as $w_i = e^{-I_i/2} / \sum_{j=1}^{n} e^{-I_j/2}$, where n is the number of fitted models. In the case of least squares case, Akaikes information is $I_i = N\log(\hat{\sigma}_i^2) + 2k_i$ for $\hat{\sigma} = \sum_{j=1}^{N} \hat{\varepsilon}_j^2 / N$, where $\hat{\varepsilon}_j$ is the estimated residuals from the fitted model and N is the number of data points. Here, the involved two

#257415 Received 14 Jan 2016; revised 2 Mar 2016; accepted 3 Mar 2016; published 7 Mar 2016

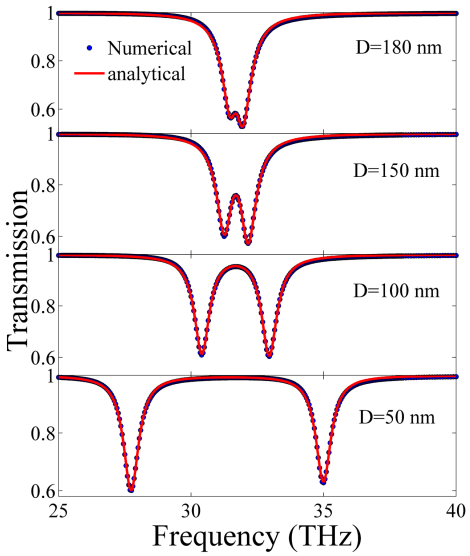

Fig. 4. Numerical (blue dots) and analytically fitted (red curves) transmission spectra for different separation of D.

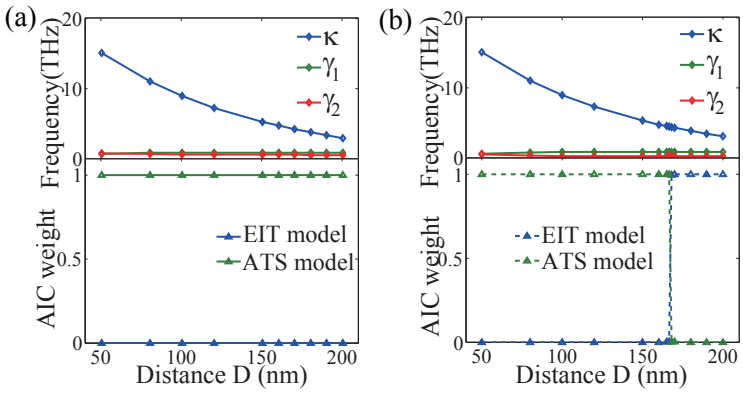

Fig. 5. (a) Upper panel: The parameters κ, γ_1 and γ_2 used in fitting. Lower panel: AIC weights of the EIT (blue curve) and ATS models (green curve). (b) The same as (a), except that μ_2=30000 cm^2/(V s) here.

models are explained as [28]

$$T_{EIT} = 1 - \frac{C_1}{(\omega-\Omega_1)^2+\Gamma_1^2} + \frac{C_2}{(\omega-\Omega_2)^2+\Gamma_2^2}, \tag{7}$$

$$T_{ATS} = 1 - \frac{C_1}{(\omega-\Omega_1)^2+\Gamma_1^2} - \frac{C_2}{(\omega-\Omega_2)^2+\Gamma_2^2}, \tag{8}$$

where Ω_i, Γ_i and C_i $(i = 1,2)$ are free parameters and represent resonant frequency, damping and strength, respectively.

Following the standard method, the AIC weights of the two models are calculated and shown in the lower panel of Fig. 5(a). Clearly, the transmission spectra are ATS-like within all fitted coupling strengths. This is related to the similar damping rates of the the LPR and FSP

#257415 Received 14 Jan 2016; revised 2 Mar 2016; accepted 3 Mar 2016; published 7 Mar 2016

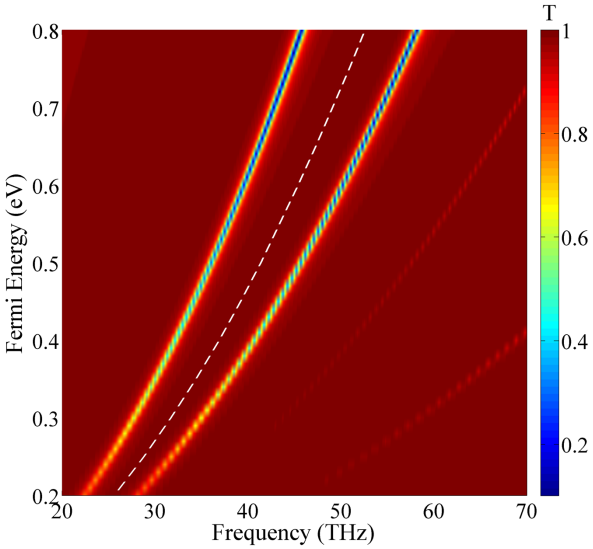

Fig. 6. Tunability of the transparency window with the change of Fermi energies E_F of graphene ribbons and sheet ($E_{F1} = E_{F2} = E_F$). D is 50 nm here. The white dashed line indicates the frequency of the LPR/FSP mode.

modes. EIT-like spectra are expected for smaller damping of the FSP mode. This is confirmed by our simulations by choosing μ_2=30000 cm^2/(V s). Corresponding fitting parameters and AIC weights are displayed in Fig. 5(b). In this case, γ_2 gets several times smaller than γ_1, as a result the spectra are EIT-like in the weak coupling region. This is consistent with the case in coupled WGM microcavities [28]. It can be further deduced that EIT is the dominant origins of transparency windows for all coupling strengths when γ_2 is far smaller than γ_1.

4. Electrical tunability

It is well known that graphene plasmons can be efficiently tuned by external voltages or chemical doping. As a result, the frequency of transparency window of our proposed PIT system can be tuned by electrically changed Fermi energy. Figure 6 displays the shift of the transparency window as Fermi energies of graphene components vary. One can see that the central frequencies of the transparency windows are kept consistent with the ones of the LPR/FSP modes, and the transparency windows broaden as the increasing of the Fermi energy of graphene. The maintenance between the agreement of the LPR and FSP modes with varied Fermi energies can be roughly understood below.

Ignoring the interactions between ribbons, the LPR resonance in suspended graphene ribbons can be described by a Fabry-Perot model [32–34]:

$$\triangle\varphi + qW = n\pi, \tag{9}$$

where integer n denotes the resonance order and $\triangle\varphi$ is the phase shift of plasmon waves on ribbon edges, which is found to be $\pi/4$ for free-standing ribbons. For the identical Fermi energy, the graphene ribbons and graphene sheet shares the same wave vector. Comparing Eq. 4 with Eq. 9 and assigning values of $m = 1, n = 1$, the resonance condition at the same frequency is expressed as $W = 3\Lambda/8$=125 nm. Thus the agreement between the LPR and FSP resonance can be maintained and is independent on E_F. This calculated width is larger than 104 nm, resulting from the redshift of spectrum when the interactions among ribbons are considered.

#257415 Received 14 Jan 2016; revised 2 Mar 2016; accepted 3 Mar 2016; published 7 Mar 2016

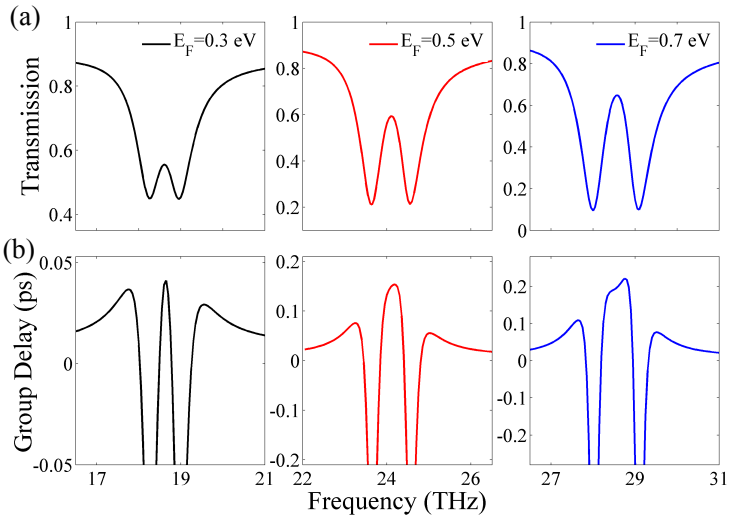

Fig. 7. (a) Transmission spectra for graphene grating-sheet system at different Fermi energies $E_F(E_{F1} = E_{F2} = E_F)$. Width of graphene ribbons is 183 nm. Distance between grating and sheet is 150 nm. (b) Corresponding group delays with increased Fermi energies.

5. Applications in slow light and electrical-optical switch

Next, to illustrate the applications of our proposed graphene PIT system, the dielectric environment is adopted as $\varepsilon_1 = 1$, $\varepsilon_2 = 2$ and $\varepsilon_3 = 4$. By redesigning the width of graphene ribbons to 183 nm, transparency windows with different Fermi energies of graphene are obtained, as shown in Fig. 7(a). The group delay times for the corresponding structures are displayed in Fig. 7(b). Positive group delay emerges at the transparency window, larger than 0.2 ps near 28.6 THz when E_F is 0.7 eV. Besides, the large group delays can be actively tuned by different Fermi energies.

Moreover, the transparency window in Fig. 7(a) arises when the graphene ribbons and sheet are tuned at identical Fermi energy. Therefore, the divergence of Fermi energies can result in degeneration and even absence of the transparency window, revealing promising applications in active electro-optical switch. As demonstrated in Fig. 8(a), when $E_{F1} = E_{F2}$=0.5 eV, transparency window emerges, thus light can pass through and have a transmission of 84% at 24.2 THz, which is ON state. While, when E_{F2} is tuned to 0.3 eV, the transparency window disappears and the corresponding transmission is at the Lorentz dip with the lowest value of 11%, which is OFF state. Moreover, as shown in Fig. 8(b) and 8(c), the switch of ON/OFF state can be tuned by changing the Fermi energies of graphene ribbons, and the ON/OFF ratio can exceed 95% at E_{F1}=0.7 eV.

6. Conclusions

In conclusion, the physical mechanisms and applications of graphene grating-sheet systems are demonstrated. Profited by the larger decay distance of the FSP mode, our PIT system relaxes the rigorous near-field coupling condition compared to previous designs. Specifically, the efficient coupling can be fulfilled at large separation of 120 nm. The response of the proposed system can be well fitted by two-oscillator model. Analysis employing AIC weight reveals that the transparency window is more like caused by ATS instead of EIT for low carrier mobility of graphene. Furthermore, EIT-like spectra are obtained for higher carrier mobility of graphene

#257415 Received 14 Jan 2016; revised 2 Mar 2016; accepted 3 Mar 2016; published 7 Mar 2016

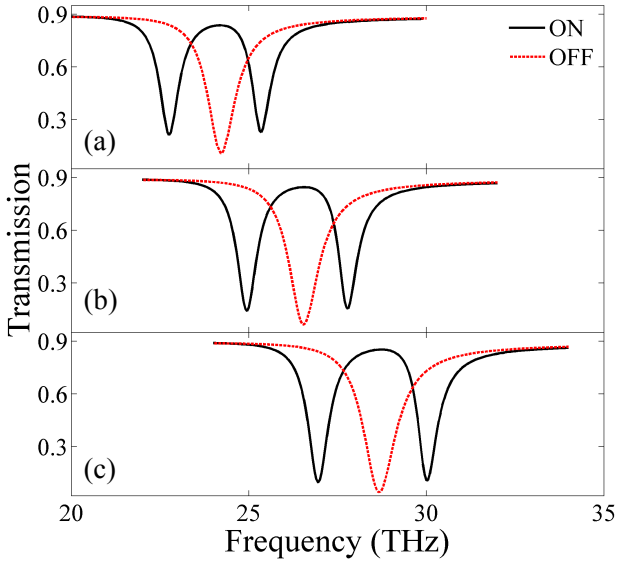

Fig. 8. The performance in active electric-optical switches. E_{F1} are (a) 0.5 eV, (b) 0.6 eV and (c) 0.7 eV, respectively. At ON states (black solid curves), E_{F2} have the identical values as E_{F1} in all three panels. While at OFF states (red dashed curves, E_{F2} are (a) 0.3 eV, (b) 0.35 eV and (c) 0.4 eV, respectively. The distance D is 100 nm.

sheet. Then applications of the hybrid system in active slow light device and electro-optical switch are also demonstrated. Large group delay emerges at the transparency window and can be electrically tuned when the Fermi energies of graphene system are changed. The unique requirement on Fermi energies of the PIT system can be utilized in active optical shutter. The ON/OFF state of the switch can be electrically controlled by changing the difference of Fermi energies between the two graphene components, and the ON/OFF ratio can exceed 95%. Moreover the work frequency of the switch can be actively tuned by changing the Fermi energy of the graphene ribbons. The proposed configuration is demonstrated as an easy-fabricated and flexibly tunable PIT system, opening up new avenues for practical applications in photonic circuits, such as sensors, slow light devices and electro-optical switches.

Acknowledgments

This work was financially supported by the National Basic Research Program of China (2013CB328702), Program for Changjiang Scholars and Innovative Research Team in University (IRT0149), the National Natural Science Foundation of China (NSFC) (11374006) and the 111 Project (B07013).

#257415 Received 14 Jan 2016; revised 2 Mar 2016; accepted 3 Mar 2016; published 7 Mar 2016